CrossMark

Gaia23bab: A New EXor

T. Giannini[1] , E. Schisano[2] , B. Nisini[1] , P. Ábrahám[3,4,5,6] , S. Antoniucci[1] , K. Biazzo[1] , F. Cruz-Sáenz de Miera[3,4,7] ,
E. Fiorellino[8] , M. Gangi[1,9] , A. Kóspál[3,4,6,10] , M. Kuhn[11] , E. Marini[1] , Z. Nagy[3,4] , and D. Paris[1]

[1] INAF—Osservatorio Astronomico di Roma, Via di Frascati, 33, 00078 Monte Porzio Catone, Italy
[2] INAF—Istituto di Astrofisica e Planetologia Spaziali, Via Fosso del Cavaliere 100, I-00133 Roma, Italy
[3] HUN-REN Research Centre for Astronomy and Earth Sciences, Konkoly Observatory, Konkoly Thege Miklós út 15-17, H-1121, Hungary
[4] CSFK, MTA Centre of Excellence, Budapest, Konkoly Thege Miklós út 15-17, H-1121, Hungary
[5] Department of Astrophysics, University of Vienna, Türkenschanzstrasse 17, A-1180 Vienna, Austria
[6] Institute of Physics and Astronomy, ELTE Eötvös Loránd University, Pázmány Péter sétány 1/A, 1117 Budapest, Hungary
[7] Institut de Recherche en Astrophysique et Planétologie, Université de Toulouse, UT3-PS, CNRS, CNES, 9 avenue du Colonel Roche, 31028 Toulouse Cedex 4,
France
[8] INAF—Osservatorio Astronomico di Capodimonte, Via Moiariello 16, I-80131 Napoli, Italy
[9] ASI, Italian Space Agency, Via del Politecnico snc, 00133 Rome, Italy
[10] Max Planck Institute for Astronomy, Königstuhl 17, 69117 Heidelberg, Germany
[11] Centre for Astrophysics Research, University of Hertfordshire, College Lane, Hatfield, AL10 9AB, UK
Received 2023 November 8; revised 2024 March 27; accepted 2024 April 1; published 2024 May 16

Abstract

On 2023 March 6, the Gaia telescope alerted a 2 mag burst from Gaia23bab, a young stellar object in the Galactic plane. We observed Gaia23bab with the Large Binocular Telescope obtaining optical and near-infrared spectra close in time to the peak of the burst, and collected all public multiband photometry to reconstruct the historical light curve. The latter shows three bursts in 10 years (2013, 2017, and 2023), whose duration and amplitude are typical of EXor variables. We estimate that, due to the bursts, the mass accumulated on the star is about twice greater than if the source had remained quiescent for the same period of time. Photometric analysis indicates that Gaia23bab is a class II source with age $\lesssim$1 Myr, spectral type G3−K0, stellar luminosity ∼4.0 $L_\odot$, and mass ∼1.6 $M_\odot$. The optical/near-infrared spectrum is rich in emission lines. From the analysis of these lines we measured an accretion luminosity and mass accretion rate ($L_{\rm acc}^{\rm burst} \sim$ 3.7 $L_\odot$, $\dot{M}_{\rm acc}^{\rm burst} \sim 2.0 \times 10^{-7}\, M_\odot\,{\rm yr}^{-1}$) consistent with those of EXors. More generally, we derived the relationships between accretion and stellar parameters in a sample of EXors. We find that, when in burst, the accretion parameters become almost independent of the stellar parameters and that EXors, even in quiescence, are more efficient than classical T Tauri stars in assembling mass.

Unified Astronomy Thesaurus concepts: Eruptive variable stars (476); Stellar accretion (1578); Pre-main sequence stars (1290); Star formation (1569)

1. Introduction

Photometric variability is a common feature of low-mass ($<2\,M_\odot$) young stellar objects (YSOs; e.g., Megeath et al. 2012). Very different timescales are involved in the observed variability: from short-term events (minutes to days) due to magnetic activity, like surface spots, stellar flares, and coronal mass ejections, up to long-term events (months to years and centuries) induced by extinction changes due to inner-disk warps, or abrupt variations in the accretion rate. To this latter class of variability events belong so-called eruptive young stars (EYSs), historically categorized as FU Orionis–type objects or FUors (Herbig 1977), and EX Lupi–type objects, or EXors (Herbig 1989). FUors present powerful outbursts of 3–6 mag in the visual band that last from several years to centuries, and take months to years to reach the peak. Their spectral type depends on the observed wavelength: F−G type in the optical to K−M type in the near-infrared (NIR; Hartmann & Kenyon 1996; Audard et al. 2014; Connelley & Reipurth 2018; Fischer et al. 2023). During the outburst, the accretion rate is of the order of 10^{-4}–$10^{-5}\,M_\odot\,{\rm yr}^{-1}$ and the spectra are dominated by absorption lines. EXor bursts have amplitudes of 1–3 mag in

the optical, last for a few months or a year, and are recurring (Fischer et al. 2023). Their spectra resemble those of K- or M-type dwarfs rich in emission lines, showing accretion rates in burst of the order of 10^{-6}–$10^{-7}\,M_\odot\,{\rm yr}^{-1}$.

A dozen EXors were classified by Herbig (1989) due to their resemblance to the prototype of the class EX Lupi. From then until the early 2000s, the number of EYS candidates just slightly increased to some tens (Audard et al. 2014) and therefore, eruptive accretion episodes were considered as peculiar and rare events. This view, however, has now been rapidly changing thanks to the discoveries of the Gaia telescope, which in eight years of operations has issued alerts[12] (Hodgkin et al. 2021) of significant photometric changes in the light curve of about 700 known or candidate YSOs. It is interesting that the vast majority of alerted sources undergo photometric variations that do not fit into the two classical EYS categories, while only a few present light curves resembling those of confirmed EXor or FUor variables. Indeed, just three sources have been claimed as bona fide FUors: Gaia17bpi (Hillenbrand et al. 2018), Gaia18dvy (Szegedi-Elek et al. 2020), and Gaia21elv (Nagy et al. 2023). To these add four further sources that share properties of FUors and EXors—Gaia19ajj (Hillenbrand et al. 2019), Gaia19bey (Hodapp et al. 2020), Gaia21bty (Siwak et al. 2023), and Gaia18cjb (Fiorellino et al. 2024)—and four EXors: Gaia18dvz (ESO-Hα99; Hodapp et al. 2019),

[12] http://gsaweb.ast.cam.ac.uk/alerts/alertsindex
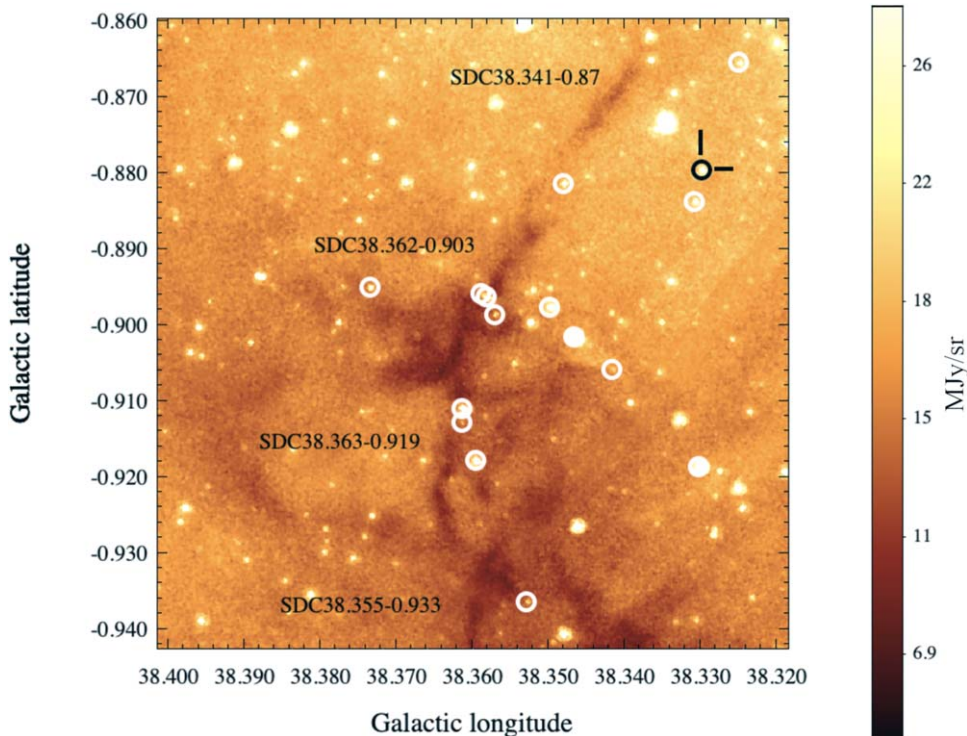
Figure 1. IRAC band 4 (8.0 μm) image of a 3×3 arcmin^2 sky area containing Gaia23bab (marked in black). White circles are YSOs of the cluster G38.3-0.9, and labels indicate the location of the Spitzer Dark Clouds from the Peretto & Fuller (2009) catalog. The surface brightness scale is given in MJy sr^{-1} in the right bar.

Gaia20eae (Hankins et al. 2020; Cruz-Sáenz de Miera et al. 2022; Ghosh et al. 2022), Gaia19fct (Miller et al. 2015; Park et al. 2022), and Gaia22dtk (Kuhn et al. 2022).

On 2023 March 6, Gaia alerted a 2 mag burst of Gaia23bab ($\alpha_{J2000.0} = 19^h04^m26^s68$, $\delta_{J2000.0} = +04°23'57''37$). Also known as SPICY 97589 (Kuhn et al. 2021), Gaia23bab is a YSO belonging to a small cluster of $\sim$30 members named G38.3-0.9. In Figure 1 we show the 3×3 arcmin^2 IRAC band 4 image of the cluster, where there are also four Spitzer Dark Clouds (Peretto & Fuller 2009), within which the cluster is partially embedded. The membership of Gaia23bab to G38.3-0.9 has been demonstrated by Kuhn et al. (2023) on the basis of the parallaxes and proper motions of six members of the cluster reported in the Gaia DR3 archive (Gaia Collaboration et al. 2016, 2021). The cluster parallax is 1.114 ± 0.056 mas, corresponding to a distance $d = 900 \pm 45$ pc.

The photometric and spectroscopic properties of Gaia23bab are the subject of the present paper. We first describe the spectroscopic observations (Section 2). Then, the photometric analysis and spectroscopic analysis are presented in Sections 3–4. A short discussion is given in Section 5, while a summary is presented in Section 6.

2. Observations and Data Reduction

We observed Gaia23bab with the 8.4 m Large Binocular Telescope (LBT) located at Mount Graham, Arizona, USA. The long-slit optical spectrum was obtained by combining the observations collected on 2023 May 28 and 29, with the Multi-object Double Spectrograph (MODS; Pogge et al. 2010). The MODS observations were done with the dual grating mode (blue + red channels, spectral range 350–950 nm) by using a $0''80$ slit ($\mathfrak{R} \sim 1500$ and 1800 in the blue and red channels, respectively). The total integration time was 1800 s. The slit

angle matched the parallactic angle to minimize the wavelength dependence of the slit transmission. During the two nights (2023 May 30 and June 1) the LBT Utility Camera in the Infrared (LUCI; Seifert et al. 2003) was used with the zJ and HK grisms to obtain the 1.0–2.4 μm spectrum. We used the G200 low-resolution grating coupled with the $0''75$ slit, corresponding to $\mathfrak{R} \sim 1500$. The observations were performed adopting the standard ABBA technique with a total integration time of 1350 s.

Data reduction was done using the Spectroscopic Interactive Pipeline and Graphical Interface (SIPGI; Gargiulo et al. 2022), specifically developed to reduce LBT long-slit spectra. The data reduction steps for each MODS spectral image were dark and bias correction, bad-pixel mapping, flat-fielding, correction for optical distortions in the spatial and spectral directions, and extraction of the one-dimensional spectrum by integrating the stellar trace along the spatial direction. The spectra of arc lamps were used for wavelength calibration. Images in the $griz$ bands (spatial scale $0''12$ px^{-1}) were obtained to derive the optical photometry of Gaia23bab and calibrate the MODS spectrum, by taking as references all stars in the field present in the Pan-STARRS (Panoramic Survey Telescope and Rapid Response System)[13] catalog (Chambers et al. 2016). We estimated $g = 18.97 \pm 0.09$ mag, $r = 17.11 \pm 0.09$ mag, $i = 15.51 \pm 0.07$ mag, and $z = 14.74 \pm 0.07$ mag. The intercalibration between the blue and red spectral segments was verified by matching the spectral range between 5300 and 5900 Å which was shared by the two channels.

The raw LUCI spectral images were corrected for bad pixels, flat-fielded, sky-subtracted, and corrected for optical distortions in both the spatial and spectral directions. Telluric lines present in the final spectrum were removed by dividing the target

---

[13] https://outerspace.stsci.edu/display/PANSTARRS/
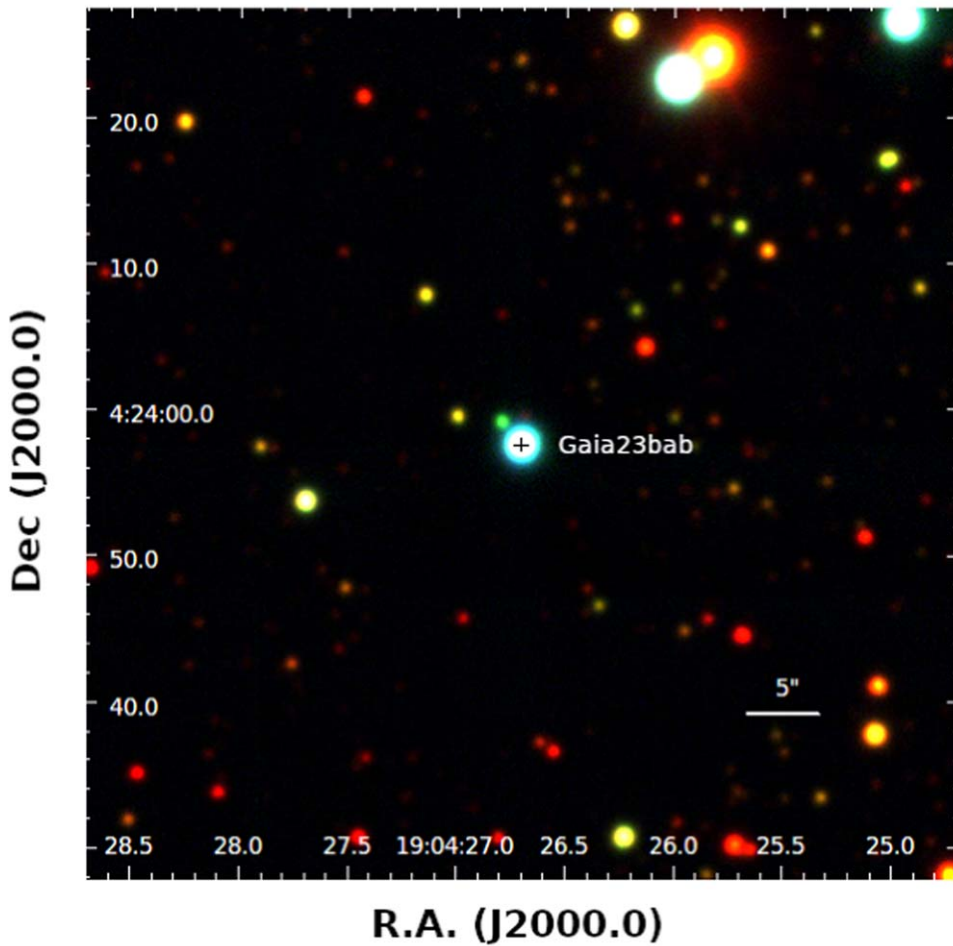
Figure 2. LBT three-color image of 1×1 arcmin^2 sky area centered on Gaia23bab. The color code is as follows: red, $J+H+K_s$ (LUCI); green, $i+z$ (MODS); blue, $g+r$ (MODS). Note that Gaia23bab is among the bluest objects in the field.

spectrum by that of a spectrophotometric standard star observed immediately after the target and corrected for intrinsic H I recombination lines in absorption. Wavelength calibration was obtained from arc lamps' spectra. J, H, and K_s images of Gaia23bab (spatial scale $0\rlap{.}''12\,\mathrm{px}^{-1}$) were acquired to flux-calibrate the zJ and HK segments. The photometry was computed based on the Two Micron All Sky Survey (2MASS)[14] magnitudes of the sources present in the image field. We obtained $J = 13.2 \pm 0.1$ mag, $H = 12.24 \pm 0.07$ mag, and $K_s = 11.47 \pm 0.07$ mag. In Figure 2 we show a composite image of a 1×1 arcmin^2 sky area around Gaia23bab obtained from all the LBT images, where the MODS g and r images are in blue, the MODS i and z images are in green, and the LUCI J, H, and K_s images are in red. Noticeably, Gaia23bab is among the bluest objects in the field.
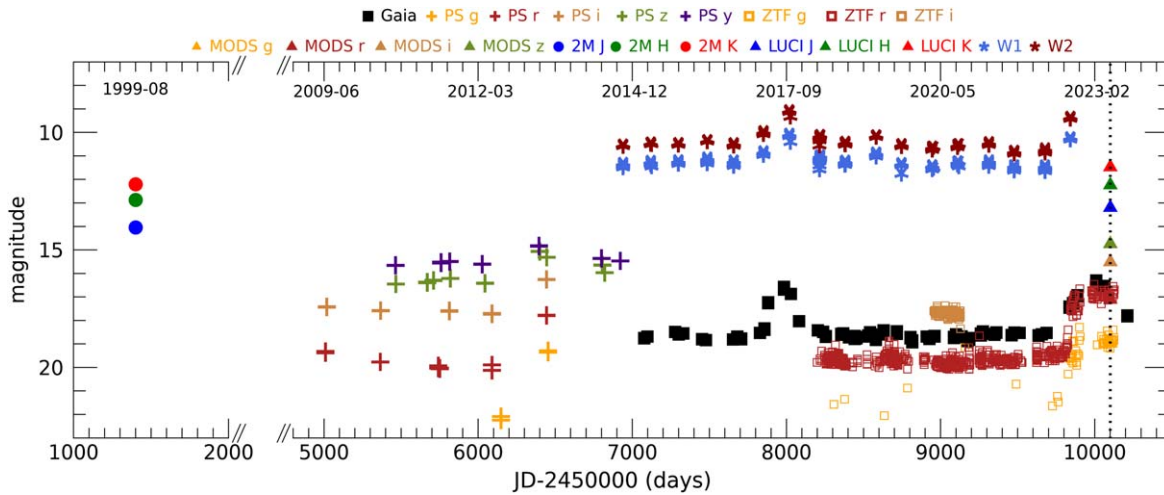
3. Photometric Analysis

3.1. Light Curve

Figure 3 shows the light curve of Gaia23bab during the last 14 years. Between 2009 and 2014 the optical photometry in the *grizy* bands was obtained within the Pan-STARRS survey, with a typical sampling of one or two points per year. The Pan-STARRS data, particularly those in the z and y bands, reveal

that a burst occurred before the advent of Gaia, roughly between 2012 April and 2014 June. A more continuous monitoring has been performed since 2014 by Gaia and, starting three years later, by the Zwicky Transient Facility (ZTF)[15] survey, which covers the *gri* bands. As already noted by Kuhn et al. (2023) the Gaia light curve shows a $\sim$2 mag burst between 2017 April and 2017 November that did not trigger a Gaia alert. Then, Gaia23bab became quiescent for about six years. During this period the photometric points in the G and r ZTF bands differ by approximately 1 mag, different from what is observed in other sources, where they roughly coincide (e.g., Cruz-Sáenz de Miera et al. 2022; Nagy et al. 2023). The offset reduces and finally disappears when Gaia23bab starts to brighten. The two filters have similar λ_{ref} (6251.5 Å and 6201.2 Å, respectively), but the G filter is broader (G-FWHM $= 4396.69$ Å, r-FWHM $= 1397.73$ Å)[16] and it extends much farther toward longer wavelengths. This suggests that if Gaia23bab is redder when fainter, it may not decrease as much in G as in r ZTF. Alternatively, the same behavior in the light curve is expected if the G flux of Gaia23bab is contaminated by that of a nearby source of similar magnitude, whose contribution becomes increasingly negligible during the burst. The ability of Gaia to resolve a nearby

---

[14] https://irsa.ipac.caltech.edu/Missions/2mass.html

[15] https://www.ztf.caltech.edu
[16] https://svo.cab.inta-csic.es/main/index.php

Figure 3. Light curve of Gaia23bab. The different symbols are the photometric points obtained within different surveys (filled squares: Gaia (*G*); crosses: Pan-STARRS; open squares: ZTF; filled circles: 2MASS; asterisks: NEOWISE; filled triangles: LBT). Different colors indicate different filters, as indicated at the top. The calendar date is indicated as well. The dotted black line marks the date of the LBT spectroscopy.

Table 1
Features of the Bursts of Gaia23bab

Burst ID	Peak Date (Calendar Date)	Instr-band	Δmag (mag)	Duration (months)	Rising Speed (mmag day^{-1})	Declining Speed (mmag day^{-1})
1	2013 Jun	Pan-STARRS-*g*	2.8	>11	9	…
1	2013 Jun	Pan-STARRS-*r*	2.1	>12	6	…
1	2013 Jun	Pan-STARRS-*i*	1.5	>12	4	…
1	2013 Jun	Pan-STARRS-*z*	1.1	25	3	2
1	2013 May	Pan-STARRS-*y*	0.8	26	3	2
2	2017 Aug	Gaia-*G*	1.8	8	14	>9
3	2023 Mar	Gaia-*G*	2.0	~12.5	7	<7
3	…	ZTF-*g*	2.8	>10	5	…
3	2023 Feb	ZTF-*r*	2.0	>10	6	<4

double star of equal luminosity is 0″23 in the along-scan direction and 0″70 in the across-scan direction, independently of the brightness of the primary (de Bruijne et al. 2015). This is higher than the ZTF's spatial sampling[17] of 1″0 px^{-1}, and therefore it is unlikely that the *G* flux is contaminated while the *r* ZTF is not. Furthermore, in both MODS and LUCI images the star closest to Gaia23bab is separated by about 2″0 (see Figure 2).

The last optical points in the light curve are the MODS *grzi* magnitudes. Our observations were obtained at the beginning of the declining phase, when the *r* ZTF magnitude was about 0.5 mag fainter than that at the burst peak.

In the infrared, Gaia23bab has been monitored since 2014 within the NEOWISE[18] survey in the W1 and W2 bands at 3.4 and 4.6 μm. The last two bursts have been registered as about 1.8 mag brightening in both bands. In Figure 3 we plot the *JHK$_s$* 2MASS and LUCI photometry, to compare the magnitudes in quiescence and burst. Their difference is $\Delta J = 0.85$ mag, $\Delta H = 0.64$ mag, and $\Delta K = 0.74$ mag.

In Table 1 we summarize the light-curve properties of the three bursts, which appear remarkably similar. First, the amplitude of each burst is always comparable to that of the others (~2 mag in *r*/*G* and ~3 mag in *g*). Second, the time elapsed between the first and the second burst is approximately

50 months, roughly the same as that between the second and the third (66 months). This frequency, together with a lack of periodicity, has been already observed in EXors (e.g., V1118 Ori, Giannini et al. 2020; ASASSN-13db, Sicilia-Aguilar et al. 2017; Gaia19fct, Park et al. 2022). Finally, we evaluated the burst rising (declining) speed in each band by fitting with straight lines the rising (declining) data in the light curve. In all cases the rising speed is some thousandths of a magnitude per day and slightly faster than the declining speed. These values are similar to those observed in V1118 Ori (Giannini et al. 2020), in Gaia20eae (Cruz-Sáenz de Miera et al. 2022), and in V2492 Cyg (Hillenbrand et al. 2013; Giannini et al. 2018).

3.2. Color–Color Diagrams

To investigate the nature of the photometric variability of Gaia23bab, we plot in Figure 4 the optical [*g* − *r*] versus [*r* − *i*] and NIR [*J* − *H*] versus [*H* − *K$_s$*] color–color diagrams for the burst and quiescence phases. In the left panel, we show the optical colors during the 2013 (Pan-STARRS, cyan dot) and 2023 (LBT, blue dot) bursts; the quiescence colors (red dot) were derived by averaging the optical photometries between 2009 and 2013. We note that the two bursts have similar colors, being both bluer with respect to quiescence by about 0.4/0.6 mag in [*g* − *r*] and 0.7/0.8 mag in [*r* − *i*]. This effect is often seen as a consequence of the dust clearing during the burst (e.g., Hillenbrand et al. 2019) and the increasing contribution to the accretion luminosity at UV wavelengths (e.g., Venuti et al.
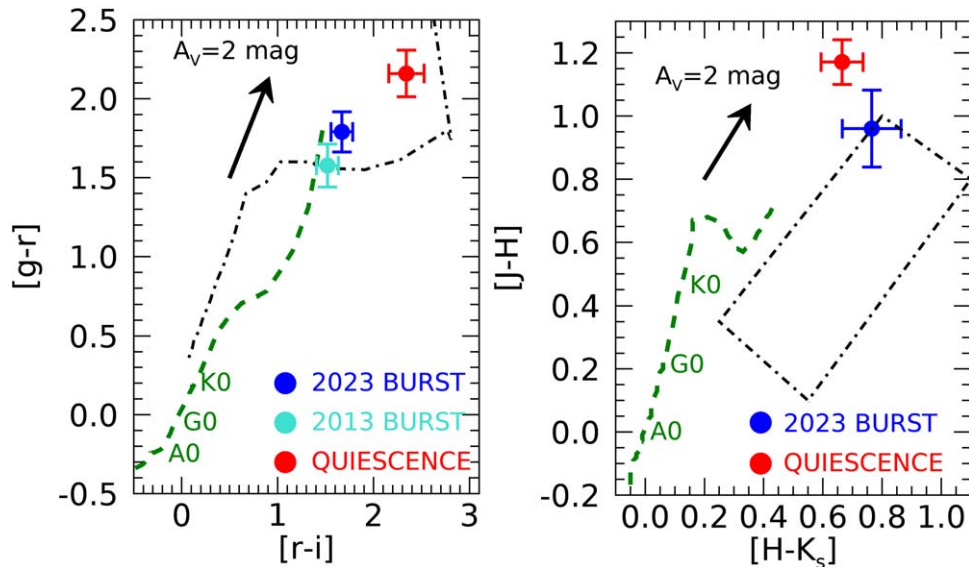
Figure 4. Left panel: two-color optical plot $[g - r]$ vs. $[r - i]$. Red and blue/cyan dots indicate quiescent points and burst points (LBT/Pan-STARRS data). The black dashed–dotted line is the locus of young stars with ages of 400–600 Myr (Kraus & Hillenbrand 2007), while the green dashed line represents the main-sequence stars with the positions of the A0, G0, and K0 spectral type stars indicated. The arrow represents the direction of the extinction vector corresponding to $A_V = 2$ mag (reddening law of Cardelli et al. 1989). Right panel: two-color NIR plot $[J - H]$ vs. $[H - K]$. Quiescent (2MASS) and burst (LUCI) data are colored red and blue, respectively. The dashed–dotted black rectangle is the locus of HAeBe stars (Hernández et al. 2005), while the green dashed line represents the main-sequence stars with the positions of the A0, G0, and K0 spectral type stars indicated. The arrow represents the direction of the extinction vector corresponding to $A_V = 2$ mag (reddening law of Cardelli et al. 1989).

2014). The colors of $400-600$ Myr young stars (Kraus & Hillenbrand 2007) and those of main-sequence stars are also plotted. Considering that the stellar spectral type is G−K (Section 3.4) we estimate an extinction of $5-6$ mag during bursts and ~ 8 mag in quiescence. In the right panel, the blue and red dots are the LUCI and 2MASS photometries, obtained more than 20 years apart. The rectangle is the locus of unreddened Herbig AeBe (HAeBe) stars of spectral type B −F (Hernández et al. 2005). Considering the error bars, the NIR colors of Gaia23bab marginally fall within this locus if dereddened by $A_V \sim 5-6$ mag in burst. Compared to those of quiescence, the colors of the burst are ~ 0.2 mag bluer in $[J - H]$ and equal within the errors in $[H - K_s]$, probably because only the internal regions of the disk are significantly heated by the burst event. This view is also supported by the approximate equality of NEOWISE colors between quiescence and burst, being $[W1 - W2]^{\mathrm{quiesc}} = 0.27 \pm 0.03$ mag and $[W1 - W2]^{\mathrm{burst}} = 0.32 \pm 0.03$ mag.

3.3. Spectral Energy Distribution

In addition to the data shown in the light curve, mid-infrared photometry of Gaia23bab is present in the Wide-field Infrared Survey Explorer (WISE) catalogs (AllWISE at 3.4, 4.6, 12.0, and 22.0 μm, and WISE Post-cryo Database at 3.4 and 4.6 μm) and in the Galactic Legacy Infrared Midplane Survey Extraordinaire (GLIMPSE),[19] which contains Spitzer IRAC photometry at 3.6, 4.5, 5.8, and 8.0 μm. The Spitzer-MIPS flux at 24 μm was taken during the MIPSGAL[20] survey and retrieved from the Gutermuth & Heyer (2014) catalog. We note that the AllWISE fluxes in the W1, W2, and W4 bands are between 0.3 and 0.6 mag brighter than the Spitzer magnitudes in the similar IRAC1, IRAC2, and MIPS1 bands. In principle,

this could be explained by the presence of sources near Gaia23bab falling in the large WISE beam. In the WISE co-added images, however, the closest star is $\sim 15''$ away in the SE direction, and thus it might slightly contaminate the Gaia23bab flux only in the W4 band, where the FHWM of the WISE beam is $12''$. A more likely explanation is that at the time of the WISE cryogenic survey (2009 December–2010 August), Gaia23bab was at a higher brightness level than it was in quiescence. This is indeed confirmed by the magnitudes in the W1 and W2 bands obtained in 2010 October during the post-cryo survey, which are all about 0.2–0.3 mag fainter than the AllWISE data. While this result is not enough for us to conclude that a burst occurred between 2009 and 2010, it is certainly evidence of Gaia23bab's mid-infrared variability.

In the far-infrared, Gaia23bab was observed within the Herschel Infrared Galactic Plane Survey (Hi-GAL) key program (Molinari et al. 2010) that surveyed the Galactic plane with the photometers PACS[21] (Photodetector Array Camera and Spectrometer) and SPIRE[22] (Spectral and Photometric Imaging REceiver) at 70, 160, 250, 350, and 500 μm. We derived the Herschel magnitudes applying both aperture and Gaussian photometry, getting reliable measurements at 160, 250, and 350 μm. At 70 μm the source is barely visible, so that we were only able to estimate an upper limit to the flux, while at 500 μm Gaia23bab is confused with the strong background emission. The spectral energy distribution (SED) is presented in Figure 5. In red and blue are shown the observed photometric points of quiescence and burst state,[23] respectively. The Pan-STARRS and ZTF points are the average values of the data in the light curve for each state. In the mid-infrared, we took the Spitzer and WISE photometries as

---
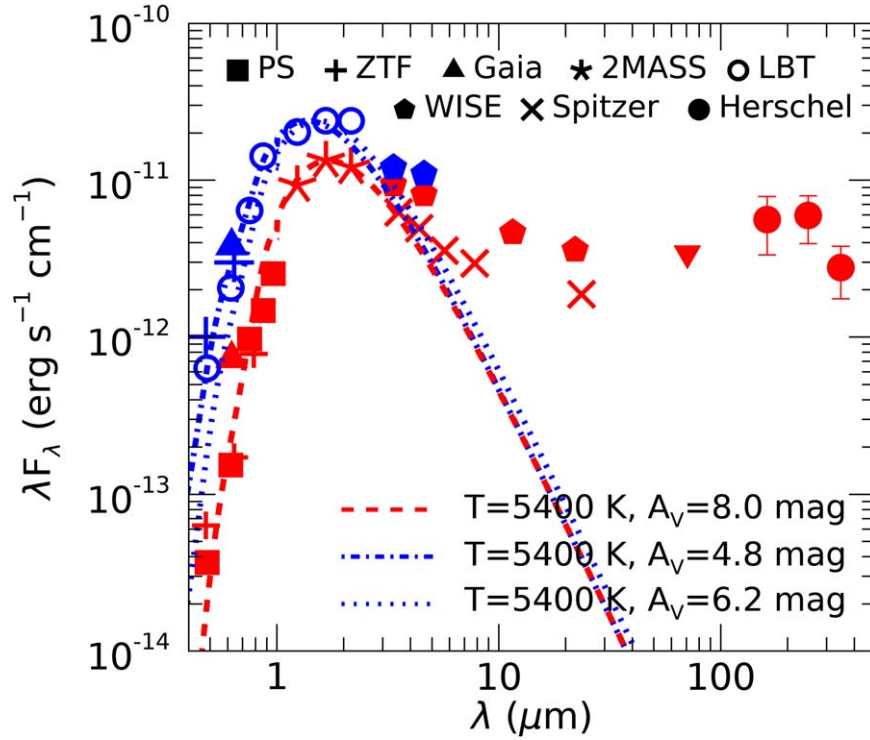
Figure 5. SED of Gaia23bab using data at different epochs. In red and blue are shown the data (not corrected for extinction) in quiescence and in burst, respectively. The down triangle is the 2σ upper limit at 70 μm. Photometric points from different catalogs are plotted with different symbols. The red and blue dashed lines are the blackbody function at $T = 5400$ K, extincted for $A_V = 8.0$ mag and 6.1 mag, respectively (see Sections 3.2, 3.4, and 4.1).

representative of the quiescence and burst phase, respectively. Furthermore, considering that the amplitude of the variability decreases with λ, for $\lambda > 24$ μm we adopted the same photometric points for computing the bolometric luminosity ($L_{\rm bol}$) in quiescence and in burst.

We first dereddened the photometries up to 24 μm with $A_V \sim 8$ mag in quiescence and A_V between 4.8 and 6.2 mag in burst, based on the estimates of the following spectroscopic analysis (Section 4.1). $L_{\rm bol}$ was then derived with the area in the plane F_λ versus λ integrated by interpolating with straight lines the SED data. A bolometric correction was applied to take into account the contribution at $\lambda > 350$ μm, considering that the emission decreases as $1/\lambda^2$. Assuming $L_{\rm bol} = L_* + L_{\rm acc}$ (L_* and $L_{\rm acc}$ being the stellar and accretion luminosity, respectively) and $d = 900$ pc, we obtained $L_{\rm bol}^{\rm quiesc} = L_* + L_{\rm acc}^{\rm quiesc} \sim 5\,L_\odot$ and $L_{\rm bol}^{\rm burst} = L_* + L_{\rm acc}^{\rm burst} = 10.3 \pm 3.9\,L_\odot$.

3.4. Stellar Properties

The stellar properties of Gaia23bab were derived through the NIR photometry and extinction in the quiescent phase. For a distance of 900 pc and $A_V = 8.0$ mag, the absolute J, H, and K_s magnitudes are 1.97, 1.67, and 1.49 mag, and the intrinsic $[J - H]$ and $[H - K_s]$ colors are 0.30 mag and 0.18 mag, respectively. Considering the tables of Pecaut & Mamajek (2013) for sources with ages between 5 and 30 Myr, the spectral type is G3−K0, and the effective temperature is $T_{\rm eff} = 5400 \pm 400$ K. In Figure 5 we plot the blackbody function at $T = 5400$ K, extincted for $A_V = 8.0$ mag (quiescence) and 4.8/6.2 mag (burst; see Section 4.1), to show the consistency with the observed photometric data. The bolometric magnitude, $M_{\rm bol}$, can be computed as $M_{\rm bol} = m(J) + 5 - 5\log_{10} d(\rm pc) + BC_J$, $m(J)$ being the intrinsic J magnitude and BC_J the bolometric correction. For a G3−K0 star BC_J is

1.08–1.30. Therefore, we get an $M_{\rm bol}$ between 3.05 mag and 3.27 mag. Then, an estimate of the stellar luminosity, L_*, can be obtained by $\log_{10} L_* = 0.4[M_{\rm bol,\odot} - M_{\rm bol}]$, where $M_{\rm bol,\odot}$ is the bolometric luminosity of the Sun, equal to 4.74 mag (Mamajek et al. 2015). This way, we get $L_* = 4.0 \pm 0.5\,L_\odot$. Therefore, having estimated as $\sim 5\,L_\odot$ the bolometric luminosity in quiescence (Section 3.3) we obtain $L_{\rm acc}^{\rm quiesc} \sim 1\,L_\odot$. Assuming blackbody emission, we determine the stellar radius to be $R_* = 1/2T_{\rm eff}^2/\sqrt{L_*/\pi\sigma}$, σ being the Stefan–Boltzmann constant. We find $R_* = 2.2 \pm 0.5\,R_\odot$.

An estimate of the evolutionary status of Gaia23bab is determined from a spectral index $\alpha = \frac{d\log(F_\lambda\lambda)}{d\log(\lambda)}$ between 2.16 and 22 μm (WISE) or 24 μm (Spitzer-MIPS). In quiescence we get $\alpha = -0.52$, while in burst $\alpha = -0.77$. Both of these determinations are in agreement with the spectral index $\alpha < -0.3$ typical of class II sources (Greene & Lada 1996). Also the Spitzer colors, $([3.6]-[4.5]) = 0.5$ and $([4.5]-[5.8]) = 0.77$, are in the range predicted for class II sources by the models of Allen et al. (2004) and Megeath et al. (2004), namely $0.0 < ([3.6]-[4.5]) < 0.7$ (0.8) and $0.4 < ([5.8]-[8.0]) < 1.0$ (1.1). An age $\lesssim 1$ Myr can be estimated by comparing L_* and $T_{\rm eff}$ with the evolutionary models of Siess et al. (2000; Figure 6), where the location of Gaia23bab is consistent with $M_* = 1.6 \pm 0.1\,M_\odot$.

4. Spectroscopic Analysis

The MODS and LUCI spectra of Gaia23bab are presented in Figure 7. The spectrum steeply rises between 3500 and 8000 Å likely because of the relevant extinction that affects Gaia23bab (Sections 3.2 and 4.1). As a consequence, in this wavelength range the spectrum is also very noisy, therefore preventing the possible detection of the continuum excess emission (Balmer

THE ASTROPHYSICAL JOURNAL, 967:41 (12pp), 2024 May 20
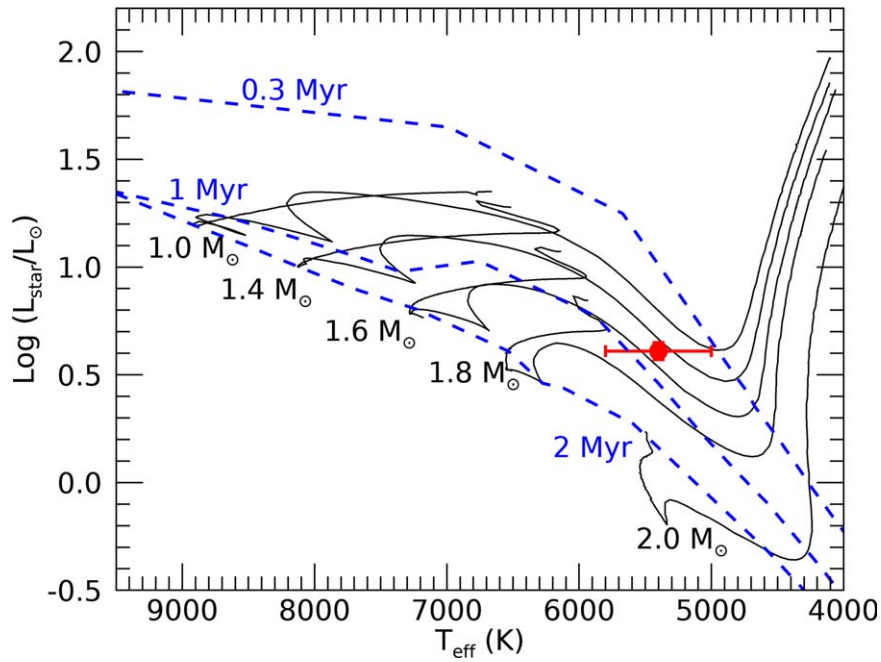
Figure 6. Evolutionary tracks of Siess et al. (2000) in the range 1–2 $M_\odot$ (black) and for ages between 0.3 and 2 Myr (blue). The red point represents Gaia23bab.
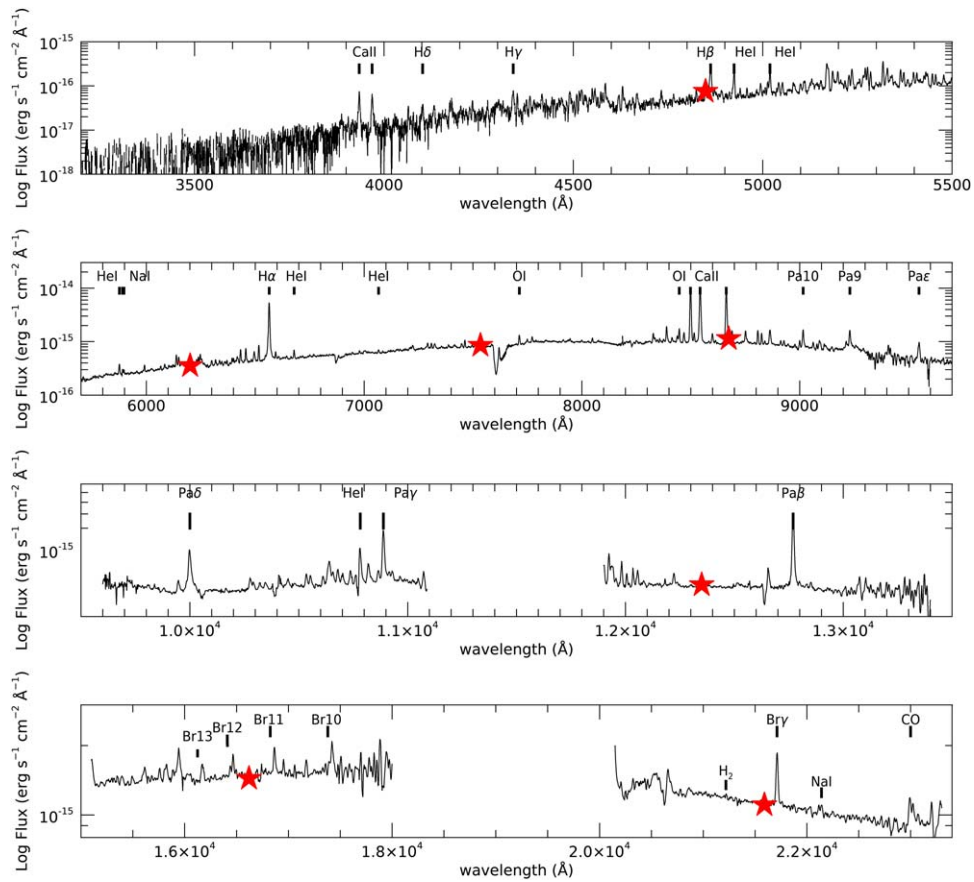
Figure 7. MODS and LUCI spectra of Gaia23bab. The photometric points in the *griz* and *JHK$_s$* bands are shown by the stars. The main spectroscopic emission lines are labeled.

jump) between 3600 and 4000 Å, which represents a direct signature of accretion (e.g., Alcalá et al. 2014 and references therein). At wavelengths between 0.9 and 1.6 μm the spectrum is almost flat and then it decreases at wavelengths longer than

2 μm, in agreement with what is expected for class II sources. A number of emission lines are detected, in particular those originating in the accretion columns, such as H I and He I recombination lines, bright Ca II and O I lines, and weaker

Table 2
Fluxes of the Main Observed Lines

Line	λ (Å)	$F \pm \Delta F$ (10^{-16} erg s^{-1} cm^{-2})
Ca II H	3934	2.6 ± 0.4
Ca II K	3968	2.3 ± 0.4
Hδ	4102	1.3 ± 0.4
Hγ	4340	2.6 ± 0.3
Hβ	4861	10.5 ± 0.6
He I	4922	5.9 ± 0.3
He I	5015	5.6 ± 0.3
He I	5875	7.0 ± 1.0
Na I	5890	2.3 ± 0.9
Na I	5896	2.6 ± 0.9
Hα	6562	299.0 ± 1.8
He I	7065	6.1 ± 2.2
O I	7774	25.1 ± 1.6
O I	8446	37.6 ± 1.7
Ca II	8498	538.9 ± 1.9
Ca II	8542	590.9 ± 1.8
Ca II	8662	507.8 ± 1.8
Pa10	9015	59.2 ± 1.8
Pa9	9229	79.1 ± 2.3
Pa8	9545	54.3 ± 1.8
Paδ	10052	230.0 ± 5.2
He I[a]	10833	(-26.1) 122.3 ± 4.5
Paγ	10941	244.2 ± 4.9
Paβ	12821	380.4 ± 4.5
Br13	16114	70.3 ± 5.2
Br12	16412	100.2 ± 7.4
Br11	16811	130.1 ± 4.1
Br10	17367	177.2 ± 6.9
H$_2$ 1-0 S(1)	21218	9.0 ± 4.0
Brγ	21661	190.0 ± 4.0
Na I	22062	18.2 ± 6.0
Na I	22090	23.2 ± 6.0
CO 2-0	22992	184.0 ± 8.8

Note. The line wavelength is in air/vacuum for $\lambda </> 1~\mu$m, respectively.
[a] In parentheses we give the flux of the absorption component of the line.

metallic lines (Alcalá et al. 2014, and references therein). In addition, emission from the disk (CO 2-0 bandhead, and Na I doublet at 2.2 μm) along with weak emission from outflowing gas (H$_2$ 1-0 S(1) 2.12 μm and He I 1.08 μm, which presents also a blueshifted absorption component) is detected. No forbidden atomic lines are present in the spectrum. Line fluxes and their 1σ errors were computed using the SPLOT task in IRAF, which takes into account both the effective readout noise per pixel and the photon noise in the spectral region containing the emission line.[24] The fluxes of the main emission lines are given in Table 2.

4.1. Extinction during Burst

A first A_V estimate of 5–6 mag for the 2023 burst has been derived from the optical/NIR color–color diagrams (Section 3.2). An independent measure is based on the ratio

---

[24] The effective readout noise per pixel was measured as the rms deviation of the continuum on either side of each line. The average rms deviation was then set as the parameter σ_0 in SPLOT. The photon noise was estimated as invgain*I, where invgain is the reciprocal of the MODS/LUCI gain (2.5/2.0 e^-/ADU expressed in physical units) and I is the pixel value. The error on the profile fit was then computed by a Monte Carlo simulation, whose iteration number nerrsample was set to 100.

of the observed continuum to a stellar template of the same spectral type as the target, artificially reddened by varying the value of A_V (Alcalá et al. 2021). The best estimate of A_V is obtained when this ratio has a flat slope. Although this method is commonly used in classical T Tauri stars, in strong accretors the observed continuum is not only affected by extinction, but can be also significantly enhanced by the excess continuum coming from hot spots in the accretion shock and from the disk. Such excess is described in terms of veiling, $r =$ Flux(excess)/ Flux(star), usually estimated by comparing the equivalent widths of the photospheric lines in the template spectrum with those in the target spectrum. In Gaia23bab, however, no photospheric lines are detected, either because deep bands/ lines are not expected in spectra of G−K type stars (Herczeg & Hillenbrand 2014) or because there is a high veiling. We can consider a reasonable range of r based on literature estimates, however. In classical T Tauri stars, between 6000 and 8000 Å r is typically between 0 and 2 (Fischer et al. 2011; Alcalá et al. 2021), but it can be $\gtrsim 3$ in strong accretors (e.g., Giannini et al. 2022). In this wavelength range r is roughly constant or decreases as a blackbody at $T \approx 8000$ K (considered as the temperature of the hot spot giving rise to the optical veiling; Fischer et al. 2011). To apply the procedure described above to compute A_V, we adopted as a first approximation a constant r between 0 and 6 and added the relative excess continuum to the stellar template prior to applying the variable reddening. We used the optical templates for stars with $T_{\rm eff} = 5000$–5800 K of Gonneau et al. (2020), and considered a grid of A_V between 0 and 20 mag, adopting the extinction law of Cardelli et al. (1989) and a total-to-selective extinction ratio $R_V = 3.1$. This way, we estimated A_V as a function of r, as shown in Figure 8. We note that for small values of r ($r \lesssim 3$), A_V decreases with r as expected if we consider that extinction effects tend to diminish the continuum, while veiling acts in the opposite direction. As r increases, particularly when the intensity of the excess continuum prevails over the stellar one, the spectral shape no longer changes, and A_V tends toward an asymptotic minimum. From this plot we derive $A_V = 5.5 \pm 0.7$ mag. Finally, we also checked how the derived A_V values change assuming that the veiling follows a blackbody law at $T = 8000$ K. The results do not change significantly with respect to the case of a constant veiling.

4.2. Accretion Properties

A rough measure of the accretion luminosity due to the 2023 burst event can be derived as $L_{\rm bol}^{\rm burst} - L_* = 6.3 \pm 3.9~L_\odot$. A more accurate method relies on the empirical relationships found by Alcalá et al. (2014, 2017) between the accretion luminosity, $L_{\rm acc}$, and the luminosities L_i of selected emission lines of gas in the accretion columns. In the optical range these relationships exist for more than 20 lines, namely the H I recombination lines of the Balmer and Paschen series from Hα to H15 and from Pa8 to Pa10, along with the He I, O I, and Ca II lines. In the NIR, there are relationships for Paδ, Paγ, Paβ, and Brγ. In the Gaia23bab spectrum there are 24 lines useful for determining $L_{\rm acc}$. For a fixed A_V, the best estimate of $L_{\rm acc}$ is that for which the dispersion among the individual $L_{{\rm acc}(i)}$ is minimized. The associated error is the combination of the uncertainties on the line fluxes and those on the relationships between $L_{\rm acc}$ and L_i (Alcalá et al. 2017). Typically, this error does not exceed a few tenths of solar luminosity, negligible
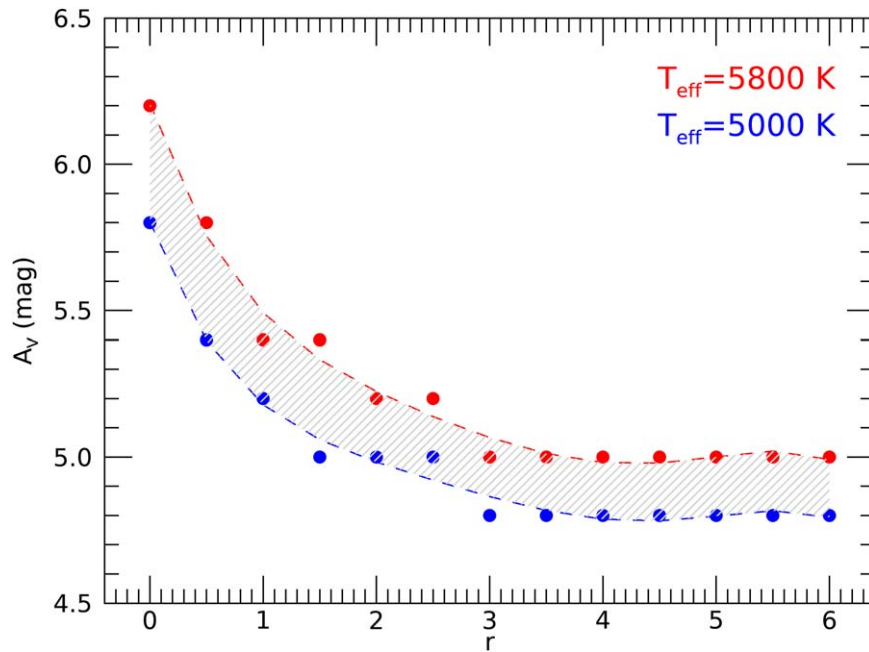
Figure 8. A_V vs. r (assumed constant) for a stellar effective temperature $T_{\rm eff}$ between 5000 and 5800 K (see Section 4.1).

with respect to that induced by the uncertainty on A_V. For $A_V = 5.5 \pm 0.7$ mag we obtain $L_{\rm acc}^{\rm burst} = 3.7 \pm 1.8\ L_\odot$.

From $L_{\rm acc}^{\rm burst}$, M_*, and R_*, we derive the mass accretion rate during the burst as $\dot{M}_{\rm acc}^{\rm burst} = (1 - R_*/R_{\rm in})^{-1}\ L_{\rm acc}^{\rm burst}\ R_*/GM_*$ (Gullbring et al. 1998), where $R_{\rm in}$ is the inner-disk radius, assumed to be $\sim 5 R_*$ (Hartmann et al. 1998), and G is the gravitational constant. We obtain $\dot{M}_{\rm acc}^{\rm burst} = (2.0 \pm 1.0)10^{-7}\ M_\odot$ yr^{-1}, in line with the mass accretion rate values found in classical EXor events (e.g., Audard et al. 2014). From the same relation, and adopting the value of $L_{\rm acc}^{\rm quiesc}$ derived in Section 3.4, we obtain $\dot{M}_{\rm acc}^{\rm quiesc} \sim 6 \times 10^{-8}\ M_\odot$ yr^{-1}. All the stellar and accretion parameters are summarized in Table 3.

5. Discussion

5.1. The Role of Bursts in Mass Assembly

One of the fundamental questions about EYSs is the role of bursts in stellar mass assembly (Fischer et al. 2023). We have estimated that during the 2023 burst, the luminosity due to accretion was comparable to the stellar luminosity (Table 3). In the last 10 years Gaia23bab has undergone three bursts, lasting approximately 1 yr each (Table 1). Furthermore, they have similar amplitude and all present a "triangular" shape in the light curve. This allows us to assume as the average value of the mass accretion rate throughout each event half the value of $\dot{M}_{\rm acc}^{\rm burst}$ measured close to the peak of the 2023 burst. We find that over the last 10 years, 3 of which were spent in burst, the mass accumulated on Gaia23bab was $\sim 1 \times 10^{-6}\ M_\odot$, roughly twice the mass that the star would have assembled if it had remained quiescent for the same period of time. Notably, this estimate is quite similar to that evaluated for the 2022 burst of EX Lupi (Cruz-Sáenz de Miera et al. 2023). Considering that the burst amplitude is thought to decrease with time (e.g., Fischer et al. 2023), we speculate that the contribution of burst

Table 3
Stellar and Accretion Properties

Stellar Properties		Accretion Properties		
L_* ($L_\odot$)	4.0 ± 0.5		Quiescence	Outburst
M_* ($M_\odot$)	1.6 ± 0.1	$L_{\rm bol}$ ($L_\odot$)	~ 5	10.3 ± 3.9
R_* ($R_\odot$)	2.2 ± 0.5	A_V (mag)	~ 8	5.5 ± 0.7
$T_{\rm eff}$ (K)	5400 ± 400	$L_{\rm acc}$ ($L_\odot$)	~ 1	3.7 ± 1.8
Spectral Type	G3–K0	$\dot{M}_{\rm acc}$ ($M_\odot$ yr^{-1})	$\sim 6 \times 10^{-8}$	$(2.0 \pm 1.0)\ 10^{-7}$

episodes to the final stellar mass could be even higher than our estimate.

5.2. Gaia23bab in the Context of EXors

In the previous sections, we have analyzed the photometric features of Gaia23bab to show their similarities with those of EXor sources. Here, we focus on the parameters derived from the emission lines, namely the accretion luminosity and the mass accretion rate. In Figure 9 we plot $L_{\rm acc}$ versus L_* and $\dot{M}_{\rm acc}$ versus M_* for a sample of 13 known EXors, both in quiescence and in burst. For comparison, the loci of accreting T Tauri stars (Alcalá et al. 2017) and of low-mass HAeBe stars (Wichittanakom et al. 2020) are shown with gray and green shaded areas, respectively. For a large majority of the sources, $L_{\rm acc}$ was measured in the same way, namely by applying the Alcalá et al. (2017) relations between optical/NIR emission lines and accretion luminosity. Both in quiescence and in burst we find a tight relation between $L_{\rm acc}$ and L_*, which spans more than 2 orders of magnitude in L_*. A good correlation is also found between $\dot{M}_{\rm acc}$ and M_* but with a larger spread that is likely due to the uncertainty in the stellar mass and radius determinations.
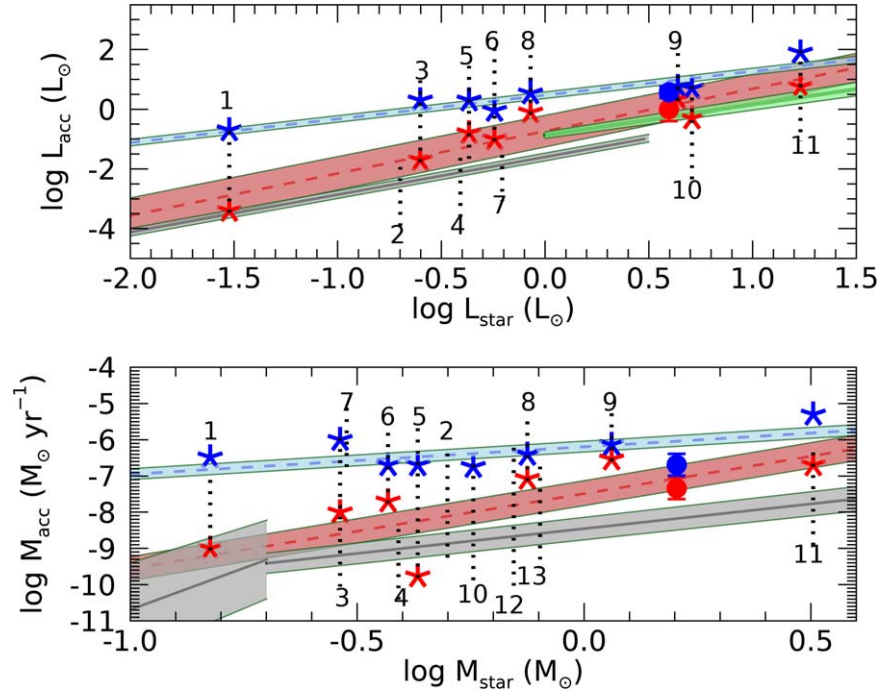
Figure 9. L_{acc} vs. L_* (top panel) and $\dot{M}_{acc}$ vs. M_* (bottom panel) in a sample of known EXors. Red and blue asterisks are the $L_{acc}/\dot{M}_{acc}$ in quiescence and in burst, respectively. The filled circles represent Gaia23bab. The red and blue dashed lines are the best linear fit through the data in quiescence and in burst and the shaded areas are the correspondent 1σ standard deviation. The gray/green solid lines are the relationships valid for classical T Tauri/low-mass HAeBe stars, and the shaded areas are the associated uncertainty (Alcalá et al. 2017; Wichittanakom et al. 2020). The individual sources were identified from the following parenthetical references: #1: ASASSN-13db (Holoien et al. 2014; Sicilia-Aguilar et al. 2017); #2: V1143 Ori (Sipos & Kóspál 2014; Giannini et al. 2022); #3: V1118 Ori (Giannini et al. 2017, 2020); #4: VY Tau (Sipos & Kóspál 2014; Giannini et al. 2022); #5: EX Lup (Aspin et al. 2010; Cruz-Sáenz de Miera et al. 2023; note that for this source, determinations of the accretion parameters for two bursts are available); #6: XZ Tau (Hartigan & Kenyon 2003; Osorio et al. 2016; Antoniucci et al. 2017; Giannini et al. 2022); #7: UZ Tau E (Yang et al. 2012; Giannini et al. 2022); #8: DR Tau (Banzatti et al. 2014; Antoniucci et al. 2017); #9: Gaia20eae (Cruz-Sáenz de Miera et al. 2022); #10: Gaia19fct (Giannini et al. 2022; Park et al. 2022); #11: PV Cep (Giannini et al. 2022 and references therein); #12: V2492 Cyg (Giannini et al. 2018); #13: V1180 Cas (Kun et al. 2011).

The linear fits through the data points are

$$\log L_{acc}^{quiesc} = (1.41 \pm 0.21)\log L_* - (0.73 \pm 0.17) \quad (1)$$

$$\log \dot{M}_{acc}^{quiesc} = (2.07 \pm 0.77)\log M_* - (7.49 \pm 0.33) \quad (2)$$

in quiescence and

$$\log L_{acc}^{burst} = (0.79 \pm 0.14)\log L_* + (0.14 \pm 0.11) \quad (3)$$

$$\log \dot{M}_{acc}^{burst} = (0.75 \pm 0.37)\log M_* - (6.19 \pm 0.15) \quad (4)$$

in burst.

The values measured in Gaia23bab during the burst are in agreement with both fits, if we take into account that our spectra have been taken at the beginning of the declining phase, when the r magnitude was already increased by about 0.5 mag with respect to the peak traced by the ZTF data in the same band (Section 3.1). Conversely, the accretion properties estimated in quiescence are consistent with the expected values. We recall that they have been indirectly derived from the SED, and thus a quiescent spectrum would be necessary to derive accurate determinations of L_{acc}^{quiesc} and $\dot{M}_{acc}^{quiesc}$. This will allow us to investigate whether a variable extinction has a role in the different brightness phases.

More generally, we note the following observations: (1) The angular coefficients of the relations derived in quiescence are consistent within the uncertainties with those of T Tauri stars. However, the intercepts differ by about an order of magnitude. If confirmed on the basis of a larger sample, this result would imply that EXors, even in quiescence, are more efficient than T

Tauri stars in accreting mass. (2) When in burst, the relations between accretion and stellar parameters become shallower, as if there were a limit to the amount of material that can be transferred from the disk to the star through the accretion columns. Given the low number of sources for which the accretion versus stellar properties have been derived, and the fact that the high-mass regime is represented only by the PV Cep data, these results need to be confirmed on a larger statistical basis.

6. Summary

In this paper we have presented LBT observations of the ~2 mag burst of Gaia23bab, a YSO alerted by Gaia in 2023 March. Our results, derived from the analysis of photometric and spectroscopic data, can be summarized as follows:

1. The multiwavelength light curve shows that Gaia23bab has had three bursts in the last 10 years. These bursts are quite similar to one another in amplitude, duration, and rising/declining speed, in line with those observed in EXors.

2. We determined the stellar properties of Gaia23bab. It is a 1.6 $M_\odot$, class II source with age $\lesssim 1$ Myr, spectral type G3−K0, and stellar luminosity 4.0 $L_\odot$. The accretion luminosity and the mass accretion rate in quiescence are $L_{acc}^{quiesc} \sim 1\,L_\odot$, and $\dot{M}_{acc}^{quiesc} \sim 6 \times 10^{-8}\,M_\odot\,yr^{-1}$.

3. The optical/NIR spectrum is rich in emission lines from which we have measured the accretion luminosity and the mass accretion rate during the burst. We get $L_{acc}^{burst} \sim 3.7$

$L_\odot$, comparable to the stellar luminosity. The mass accretion rate close to the burst peak is $\dot{M}_{\mathrm{acc}}{}^{\mathrm{burst}} \sim 2.0 \times 10^{-7}\ M_\odot\ \mathrm{yr}^{-1}$.

4. The mass accumulated on Gaia23bab in the last 10 years is roughly twice the mass that it would have assembled if it had remained quiescent for the same period of time.

5. Both the accretion luminosity and mass accretion rate of Gaia23bab are consistent with those of confirmed EXors.

As a more general result, we have quantified the correlations, both in quiescence and in burst, between accretion and stellar parameters in a sample of 13 EXors. On average, the EXors have L_{acc} and $\dot{M}_{\mathrm{acc}}$ larger than T Tauri stars have in the same range of mass, even in quiescence. If confirmed on the basis of a larger sample, this result would imply that EXors are more efficient than T Tauri stars in accreting mass. Also, when in burst, the accretion luminosity and mass accretion rate become poorly dependent on the central star properties.

ORCID iDs

T. Giannini ⬤ https://orcid.org/0000-0002-7035-8513
E. Schisano ⬤ https://orcid.org/0000-0003-1560-3958
B. Nisini ⬤ https://orcid.org/0000-0002-9190-0113
P. Ábrahám ⬤ https://orcid.org/0000-0001-6015-646X
S. Antoniucci ⬤ https://orcid.org/0000-0002-0666-3847
K. Biazzo ⬤ https://orcid.org/0000-0002-1892-2180
F. Cruz-Sáenz de Miera ⬤ https://orcid.org/0000-0002-4283-2185
E. Fiorellino ⬤ https://orcid.org/0000-0002-5261-6216
M. Gangi ⬤ https://orcid.org/0000-0002-8364-7795
A. Kóspál ⬤ https://orcid.org/0000-0001-7157-6275
M. Kuhn ⬤ https://orcid.org/0000-0002-0631-7514
E. Marini ⬤ https://orcid.org/0000-0002-6894-1267
Z. Nagy ⬤ https://orcid.org/0000-0002-3632-1194
D. Paris ⬤ https://orcid.org/0000-0002-7409-8114

References

Alcalá, J. M., Gangi, M., Biazzo, K., et al. 2021, A&A, 652, A72
Alcalá, J. M., Manara, C. F., Natta, A., et al. 2017, A&A, 600, A20
Alcalá, J. M., Natta, A., Manara, C. F., et al. 2014, A&A, 561, A2
Allen, L. E., Calvet, N., D'Alessio, P., et al. 2004, ApJS, 154, 363
Antoniucci, S., Nisini, B., Biazzo, K., et al. 2017, A&A, 606, A48
Aspin, C., Reipurth, B., Herczeg, G. J., et al. 2010, ApJL, 719, L50
Audard, M., Ábrahám, P., Dunham, M. M., et al. 2014, in Protostars and Planets VI, ed. H. Beuther (Tucson, AZ: Univ. of Arizona Press), 387
Banzatti, A., Meyer, M. R., Manara, C. F., et al. 2014, ApJ, 780, 26
Cardelli, J. A., Clayton, G. C., & Mathis, J. S. 1989, ApJ, 345, 245
Chambers, K. C., Magnier, E. A., Metcalfe, N., et al. 2016, arXiv:1612.05560
Connelley, M. S., & Reipurth, B. 2018, ApJ, 861, 145
Cruz-Sáenz de Miera, F., Kóspál, Á., Ábrahám, P., et al. 2022, ApJ, 927, 125
Cruz-Sáenz de Miera, F., Kóspál, Á., Abrahám, P., et al. 2023, A&A, 678, A88
de Bruijne, J. H. J., Allen, M., Azaz, S., et al. 2015, A&A, 576, A74
Fiorellino, E., Abraham, P., Kospal, A., et al. 2024, ApJ, in press
Fischer, W., Edwards, S., Hillenbrand, L., et al. 2011, ApJ, 730, 73
Fischer, W. J., Hillenbrand, L. A., Herczeg, G. J., et al. 2023, in Protostars and Planets VII, ed. S.-I. Inutsuka et al. (San Francisco, CA: ASP), 355
Gaia Collaboration, Brown, A. G. A., Vallenari, A., et al. 2021, A&A, 649, A1
Gaia Collaboration, Prusti, T., de Bruijne, J. H. J., et al. 2016, A&A, 595, A1
Gargiulo, A., Fumana, M., Bisogni, S., et al. 2022, MNRAS, 514, 2902
Ghosh, A., Sharma, S., Ninan, J. P., et al. 2022, ApJ, 926, 68
Giannini, T., Antoniucci, S., Lorenzetti, D., et al. 2017, ApJ, 839, 112
Giannini, T., Giunta, A., Gangi, M., et al. 2022, ApJ, 929, 129
Giannini, T., Giunta, A., Lorenzetti, D., et al. 2020, A&A, 637, A83
Giannini, T., Munari, U., Antoniucci, S., et al. 2018, A&A, 611, A54
Gonneau, A., Lyubenova, M., Lançon, A., et al. 2020, A&A, 634, A133
Greene, T. P., & Lada, C. J. 1996, AJ, 112, 2184
Gullbring, E., Hartmann, L., Briceño, C., et al. 1998, ApJ, 492, 323
Gutermuth, R. A., & Heyer, M. H. 2014, AAS Meeting Abstracts, 223, 336.05
Hankins, M., Hillenbrand, L. A., De, K., et al. 2020, ATel, 13902
Hartigan, P., & Kenyon, S. J. 2003, ApJ, 583, 334
Hartmann, L., Calvet, N., Gullbring, E., et al. 1998, ApJ, 495, 385
Hartmann, L., & Kenyon, S. J. 1996, ARA&A, 34, 207
Herbig, G. H. 1977, ApJ, 217, 693
Herbig, G. H. 1989, ESO Conf. and Workshop Proc., 33, 233
Herczeg, G. J., & Hillenbrand, L. A. 2014, ApJ, 786, 97
Hernández, J., Calvet, N., Hartmann, L., et al. 2005, AJ, 129, 856
Hillenbrand, L. A., Contreras Peña, C., Morrell, S., et al. 2018, ApJ, 869, 146
Hillenbrand, L. A., Miller, A. A., Covey, K. R., et al. 2013, AJ, 145, 59
Hillenbrand, L. A., Reipurth, B., Connelley, M., et al. 2019, AJ, 158, 240
Hodapp, K. W., Denneau, L., Tucker, M., et al. 2020, AJ, 160, 164
Hodapp, K. W., Reipurth, B., Pettersson, B., et al. 2019, AJ, 158, 241
Hodgkin, S. T., Harrison, D. L., Breedt, E., et al. 2021, A&A, 652, A76
Holoien, T. W.-S., Prieto, J. L., Stanek, K. Z., et al. 2014, ApJL, 785, L35
Kraus, A. L., & Hillenbrand, L. A. 2007, AJ, 134, 2340
Kuhn, M. A., Benjamin, R. A., Ishida, E. E. O., et al. 2023, RNAAS, 7, 57
Kuhn, M. A., de Souza, R. S., Krone-Martins, A., et al. 2021, ApJS, 254, 33
Kuhn, M. A., Hillenbrand, L. A., Connelley, M. S., et al. 2022, ATel, 15721
Kun, M., Szegedi-Elek, E., Moór, A., et al. 2011, ApJL, 733, L8
Mamajek, E. E., Torres, G., Prsa, A., et al. 2015, arXiv:1510.06262
Megeath, S. T., Allen, L. E., Gutermuth, R. A., et al. 2004, ApJS, 154, 367
Megeath, S. T., Gutermuth, R., Muzerolle, J., et al. 2012, AJ, 144, 192
Miller, A. A., Hillenbrand, L. A., Bilgi, P., et al. 2015, ATel, 7428
Molinari, S., Swinyard, B., Bally, J., et al. 2010, A&A, 518, L100
Nagy, Z., Park, S., Ábrahám, P., et al. 2023, MNRAS, 524, 3344
Osorio, M., Macías, E., Anglada, G., et al. 2016, ApJL, 825, L10
Park, S., Kóspál, Á., Ábrahám, P., et al. 2022, ApJ, 941, 165
Pecaut, M. J., & Mamajek, E. E. 2013, ApJS, 208, 9
Peretto, N., & Fuller, G. A. 2009, A&A, 505, 405
Pogge, R. W., Atwood, B., Brewer, D. F., et al. 2010, Proc. SPIE, 7735, 77350A
Seifert, W., Appenzeller, I., Baumeister, H., et al. 2003, Proc. SPIE, 4841, 962
Sicilia-Aguilar, A., Oprandi, A., Froebrich, D., et al. 2017, A&A, 607, A127
Siess, L., Dufour, E., & Forestini, M. 2000, A&A, 358, 593

Sipos, N., & Kóspál, Á. 2014, in IAU Proc. 299, Exploring the Formation and Evolution of Planetary Systems (Cambridge: Cambridge Univ. Press), 121

Siwak, M., Hillenbrand, L. A., Kóspál, Á., et al. 2023, MNRAS, 524, 5548

Szegedi-Elek, E., Ábrahám, P., & Wyrzykowski, Ł. 2020, ApJ, 899, 130

Venuti, L., Bouvier, J., Flaccomio, E., et al. 2014, A&A, 570, A82

Wichittanakom, C., Oudmaijer, R. D., Fairlamb, J. R., et al. 2020, MNRAS, 493, 234

Yang, H., Herczeg, G. J., Linsky, J. L., et al. 2012, ApJ, 744, 121